




Cite this: DOI: 10.1039/d5ta02824h

# Photo-swing CO<sub>2</sub> capture using a branched polyethylenimine as sorbents and TiN light absorber

Noemi Leick, <sup>\*a</sup> Sawyer Halingsstad, <sup>a</sup> James M. Crawford, <sup>ab</sup>  
G. Michael Carroll, <sup>a</sup> Matthew M. Yung, <sup>a</sup> Randy Cortright <sup>a</sup>  
and Wade A. Braunecker <sup>\*a</sup>

Using branched polyethylenimine as the sorbent material for dilute CO<sub>2</sub> capture, a photo-swing method is demonstrated in an industrially relevant support architecture using titanium nitride (TiN) nanosized light absorbers coupled with low-power LEDs with irradiances up to 420 mW cm<sup>-2</sup>. The photo-swing desorption process is applied to dry and humid streams of 400 ppm CO<sub>2</sub> diluted in N<sub>2</sub>. Consistent with known sorption mechanisms for aminopolymers, humid CO<sub>2</sub> streams increased the CO<sub>2</sub> uptake, in our case by ~30%. The photo-swing CO<sub>2</sub> capture desorbed ~83% and ~100% CO<sub>2</sub> compared to thermally-driven desorption over the same period for a dry and humid CO<sub>2</sub> stream, respectively. The photo-swing CO<sub>2</sub> capture exhibits robust performance over >90 cycles without significant signs of photo(thermal) induced sorbent degradation. This work lays the groundwork for photo-swing DAC technology as a scalable, energy-efficient solution for CO<sub>2</sub> capture, well-suited for modular systems in remote locations utilizing intermittent renewable energy sources.

Received 9th April 2025

Accepted 29th July 2025

DOI: 10.1039/d5ta02824h

[rsc.li/materials-a](https://rsc.li/materials-a)

## 1. Introduction

In the pursuit of achieving the ambitious target of reducing atmospheric carbon dioxide (CO<sub>2</sub>) levels to 350 ppm by 2100,<sup>1</sup> even after comprehensive decarbonization efforts across various sectors, managing residual CO<sub>2</sub> from industrial activities will remain a challenge. Various approaches will need to be adopted, ranging from reforestation efforts to direct air capture (DAC) technologies. While DAC is still an emerging field, there are pilot and commercial plants actively removing CO<sub>2</sub> from the atmosphere, such as Climeworks (Iceland), Zero Carbon Systems (USA), Holocene (USA), Mission Zero (United Kingdom), Avnos (USA), Verdox (USA), Heirloom (USA), and Carbon Engineering (Canada). These removal solutions mainly rely on a liquid solvent or solid sorbent acting as the CO<sub>2</sub> capture agent, which are amongst the most commercially mature material approaches.<sup>2</sup> Traditional thermal-swing adsorption methods, requiring (waste) heat for sorbent regeneration, have been a mainstay, but recent innovations are introducing novel techniques with potential energy efficiency improvements. For instance, recent research has leveraged the sublimation point of CO<sub>2</sub> that forms a solid at -78.5 °C in cryogenic DAC,<sup>3-6</sup> using moisture to release the bound CO<sub>2</sub> in moisture-swing adsorption,<sup>7-9</sup> and utilizing microwave, electric

or electrochemical desorption of CO<sub>2</sub> in electro-swing adsorption.<sup>10-15</sup> While these novel techniques harbor meaningful improvements in energy efficiency, they also use new families of materials that may delay their broader market adoption.

This study introduces a novel photo-swing adsorption solution, utilizing a readily available liquid aminopolymer, branched polyethylenimine (PEI, Mw ~800), sorbent embedded in an industrially relevant support made of a high surface area mesoporous oxide with a proprietary composition. Unlike previous reports on photocatalytic CO<sub>2</sub> capture,<sup>16-18</sup> our approach integrates an amine-containing sorbent with an earth-abundant plasmonic light absorber, specifically titanium nitride (TiN). This unique system achieves fast CO<sub>2</sub> desorption rates even at low irradiances (as low as ~50 mW cm<sup>-2</sup>, but optimized near ~420 mW cm<sup>-2</sup>), presenting compatibility with renewable energy sources and eliminating the need for co-located industrial waste heat. Notably, the modularity of the photo-swing adsorption system,<sup>2</sup> coupled with its potential compatibility with intermittent renewable grids, addresses some scalability concerns while also promoting equitable distribution of carbon capture technologies.

Photocatalysis encompasses many charge-generation and transfer mechanisms as well as photothermal mechanisms. Plasmonics is an emerging field of photocatalysis based in the concept that nanoparticles, most commonly noble metals, can be light “activated” when illuminated at their plasmonic resonance frequency, which is dependent on the material, size and morphology.<sup>19-22</sup> While the precise mechanism is not fully

<sup>a</sup>National Renewable Energy Laboratory, Golden, CO 80401, USA. E-mail: [noemi.leick@nrel.gov](mailto:noemi.leick@nrel.gov)

<sup>b</sup>Montana State University, Bozeman, MT 59717, USA



explored in detail in this study, we focus on the photothermal activation of TiN when illuminated with red light (625 nm), UV light (385 nm), and a broad-spectrum white light LED, all capable of activating TiN and titanium oxynitride ( $\text{TiO}_x\text{N}_y$ ). TiN is of particular interest as it is one of the only non-noble metal plasmonic materials that is earth abundant, has optical properties similar to gold, and remains structurally stable and plasmonically active even when partially oxidized.<sup>23–26</sup> This photo-swing process offers significant benefits in terms of scalability, modularity, and applicability across diverse environmental conditions, while also laying the foundation for future advancements in photoreactive carbon capture and conversion to value-added products.<sup>27</sup>

## 2. Materials and methods

### 2.1. Materials

The support material, referred to as “contactor”, was impregnated with branched PEI (Mw ~800) using a proprietary process similar to that from a patent.<sup>28</sup> TiN nanoparticles (NPs) were drop-cast onto the contactor from a mixture of 1 mL methanol, 5  $\mu\text{L}$  of PEI, and 10 mg TiN. The additional PEI improved the suspension of TiN in methanol and enhanced its adhesion to the contactor. The resulting contactor system consisted of 2.5 wt% TiN and ~12 wt% PEI, the latter verified by thermogravimetric analysis using published methods.<sup>29</sup> While studies highlighting proof-of-concept results employ mesoporous oxide supports with high PEI loadings (40–60 wt%), the industrial contactors used in this work incorporate additional binder materials to provide the mechanical strength and macroscopic form factor necessary for commercial-scale monolithic devices. This structural requirement reduces the overall PEI weight fraction but results in a material that is more durable and representative of deployable DAC systems.

The TiN NPs were acquired from US Research Nanomaterials, Inc. A transmission electron microscopy image (SI, Fig. S1) reveals a heterogeneous morphology and an average size distribution centered ~20 nm, with a broad absorption spectrum from 380–750 nm obtained from diffuse reflectance UV-Vis absorption spectroscopy. Once TiN was added to the samples, they were uniformly black, such that TiN is likely in excess.

Dilute streams of  $\text{CO}_2$  were obtained as cylinders of premixed 400 ppm  $\text{CO}_2$  in  $\text{N}_2$  from Matheson and humidified by diverting the gas flow through a deionized water bubbler. A flow of 100 sccm was chosen and regulated through a mass flow controller, as illustrated in Fig. 1 and photographed in Fig. S2.

### 2.2. $\text{CO}_2$ adsorption-desorption characterization

The benchtop flow-through reactor employed a standard quartz cuvette with a 1 cm pathlength.  $\text{CO}_2$  rich gas was flowed over a 0.5  $\text{cm}^2$  piece of contactor placed at the bottom of the cuvette. The gas at the outlet was analyzed using the in-line LI-COR®-850 infrared sensing system specifically tuned for low-concentration  $\text{CO}_2$  flow and for  $\text{H}_2\text{O}$  sensing. The LI-COR® sensor was used to establish saturation of  $\text{CO}_2$  as well as  $\text{H}_2\text{O}$  which reached 100%

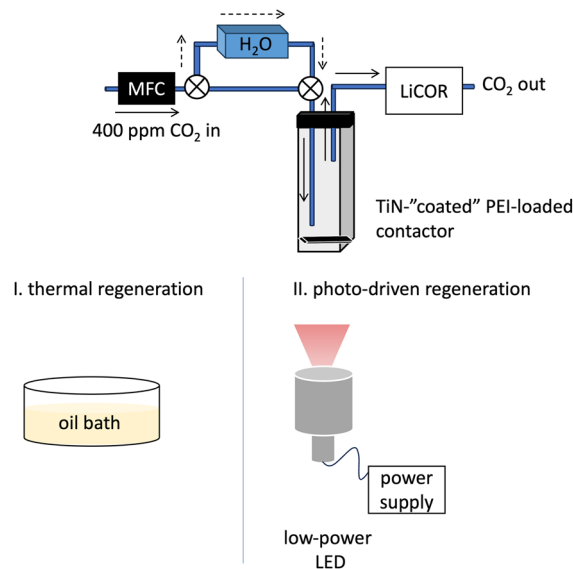


Fig. 1 Schematic representation of the experimental flow-through reactor employed in this work. A flow of 100 sccm of 400 ppm  $\text{CO}_2$  in  $\text{N}_2$  is introduced in a quartz cuvette hosting a flat piece of the PEI-loaded contactor “coated” with TiN powder. The  $\text{CO}_2$  stream can also be diverted to a water bubbler to simulate 100% relative humidity. The gas flow exiting the septum-capped cuvette passes through an infrared detector calibrated for  $\text{CO}_2$  and  $\text{H}_2\text{O}$  signals, the LI-COR®-850 detector. In this study, two methods of amine-regeneration were used: thermal regeneration, where the cuvette is immersed into an oil bath at  $T \sim 110^\circ\text{C}$ , or photo-driven regeneration. The main body of research was conducted using LEDs (300–400  $\text{mW cm}^{-2}$ ) centered at ~625 nm, ~385 nm, or a broad-spectrum white LED. The focus length from the LED to the sample is 20 cm.

relative humidity within ~30 min. Unless otherwise stated, the  $\text{CO}_2$  adsorption step was conducted for 15 min, followed by 5 min of bulk heat using an oil bath at  $110^\circ\text{C}$ , or 5 min of localized heat using LEDs. Low-power LEDs from Thorlabs were mainly used for this study, including 625 nm (red light), 385 nm (UV light), and a broadband white light, with maximum input current of 1000 mA, 700 mA, and 1000 mA, respectively. Their emission spectra can be found in Fig. S3. A focusing lens was attached to the LEDs whose focal length is 20 cm from the LED. The light was focused to a ~1 cm diameter circle on one side of the flat piece of contactor. Using a Thorlabs wireless power meter PM160T, we measured the irradiances at different set currents for the monochromatic LEDs and summarized the results in Table S1.

## 3. Results and discussion

### 3.1 Photo-induced heating compatibility with PEI

Because PEI starts experiencing thermal degradation at  $120\text{--}135^\circ\text{C}$  in dry conditions,<sup>30,31</sup> it is crucial to keep the composite below this temperature to ensure compatibility of plasmonic heating induced by the light-activation of TiN with the amino-polymer. To this end, the temperature profiles of illuminated TiN at different set currents to obtain different irradiances, as shown in Fig. 2 and Table S2, using a FLIR E6 infrared (IR)



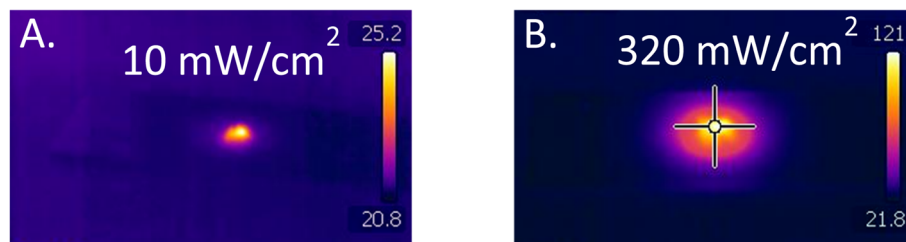


**Fig. 2** Thermal imaging of 10 mg TiN powder on glass slide in  $N_2$  atmosphere glovebox, illuminated at 625 nm perpendicular to the sample, at 23 mA input current with a measured irradiance of  $10 \text{ mW cm}^{-2}$  in (A), and at 700 mA input current with a measured irradiance of  $320 \text{ mW cm}^{-2}$  in (B). The sliding scale is different for each image, representing the minimum and maximum temperature measured in  $^{\circ}\text{C}$ .

camera. When a low irradiance is used,  $10 \text{ mW cm}^{-2}$  shown in Fig. 2A, the bulk sample temperature measured after 2 min is  $26^{\circ}\text{C}$ , while an irradiance of  $320 \text{ mW cm}^{-2}$  resulted in a measured sample temperature of  $120^{\circ}\text{C}$ . Illuminating the contactor pieces with the 625 nm LED, with a set current of 1000 mA (equivalent to  $420 \text{ mW cm}^{-2}$ ), and focused 20 cm from the

LED, the pristine contactor without TiN only reaches  $\sim 31^{\circ}\text{C}$ , while the temperature of the illuminated TiN-coated contactor rises to  $110^{\circ}\text{C}$ . Because TiN is dispersed and mixed with PEI in the TiN-contactor system, it is expected that the powder of NP-only gives rise to a higher temperature. However, the pristine contactor system has a high IR emissivity ( $\sim 0.8\text{--}0.95$ ), and we

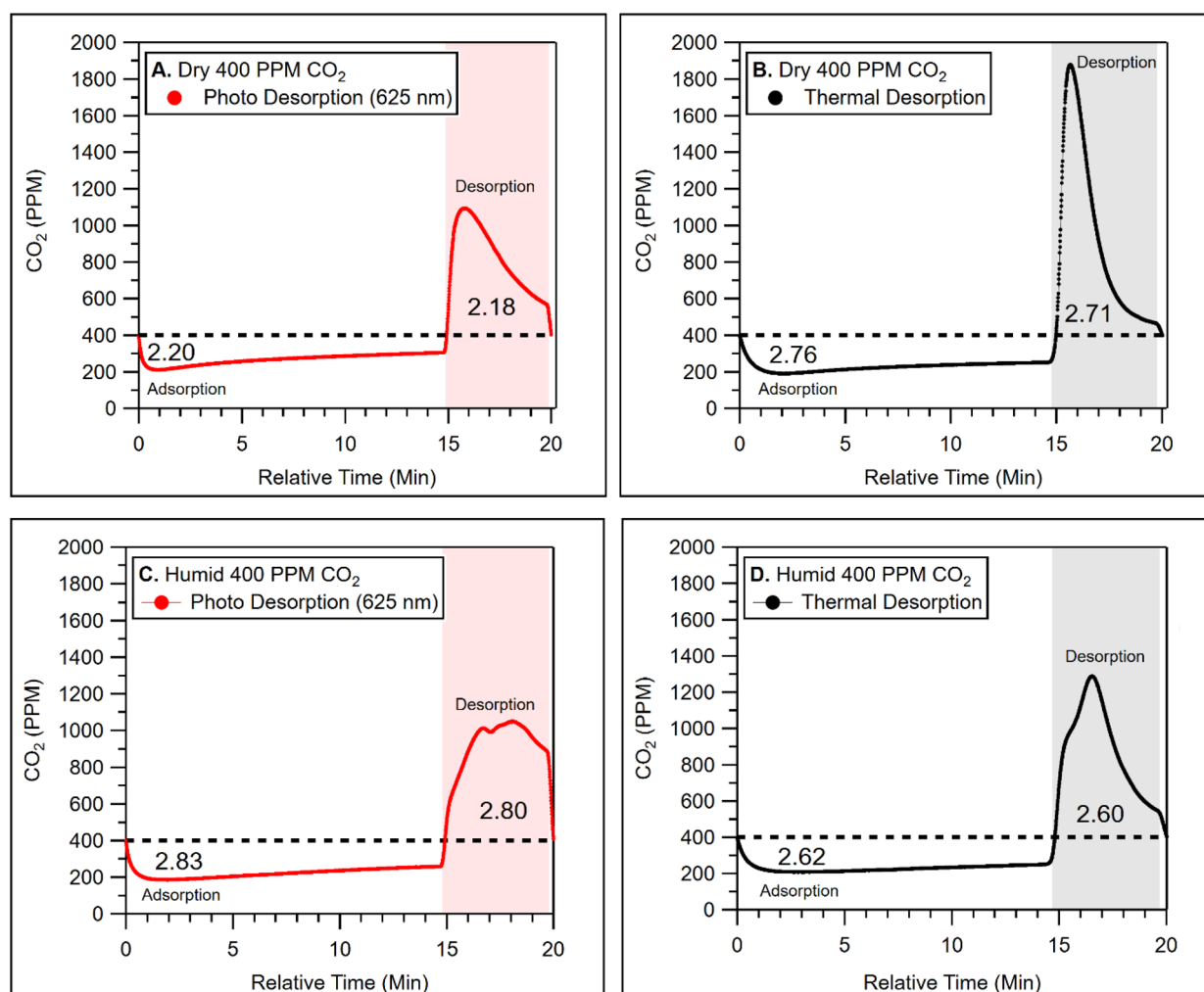


**Fig. 3**  $\text{CO}_2$  concentration (in ppm) using a flow-through reactor with 15 min adsorption time and 5 min exposure to 625 nm-light at irradiances of  $\sim 420 \text{ mW cm}^{-2}$  (red trace in (A) and (C)) or an oil bath at  $T \sim 110^{\circ}\text{C}$  (black trace in (B) and (D)), for dry  $\text{CO}_2$  flow ((A) and (B)) and humid  $\text{CO}_2$  flow ((C) and (D)). The dashed line is a guide to eye for the baseline  $\text{CO}_2$  concentration of 400 ppm. The value in the adsorbed and desorbed portion of the signal is the integrated area (in  $\text{mmol CO}_2$  per g PEI) representing the amount of  $\text{CO}_2$  desorbed. The conversion between ppm of  $\text{CO}_2$  to  $\text{mmol CO}_2$  per g PEI can be found in Section S5. For these experiments, the same TiN-impregnated contactor system was used.



expect the measured temperature of the composite system  $\sim 110^\circ\text{C}$  to be more accurate, and therefore the photo-induced heating to be compatible with the stability window of PEI. While the plasmonic community often debates the extent to which different catalytic mechanisms are influenced by charge transfer (also known as hot electrons), plasmon induced resonant energy transfer, or thermal effects,<sup>32–35</sup> in this study we do not attempt to disentangle potential contribution from these mechanisms. However, it is likely that the light activates the plasmonically active TiN nanoparticles and simply induces local collective heating at the microscale that results in the desorption of  $\text{CO}_2$ .<sup>36–38</sup>

### 3.2 Effluent measurements of $\text{CO}_2$ desorption in humid and dry conditions: photo-*vs.* temperature-swing desorption

We monitored the  $\text{CO}_2$  concentration in line with the cuvette-reactor depicted in Fig. 1, while constantly flowing 400 ppm  $\text{CO}_2$  diluted in  $\text{N}_2$ , and desorbing  $\text{CO}_2$  using light or applied heat. Fig. 3 shows the resulting profile for the photo-swing and temperature-swing desorption under dry (Fig. 3A and B, respectively) and humid  $\text{CO}_2$  flow (Fig. 3C and D, respectively), with desorption marked by the shaded areas. After 15 min of adsorption, though the sorbent was not yet saturated,  $\text{CO}_2$  desorption was triggered. It is common practice with composite sorbent systems not to fully saturate PEI, but rather utilize  $\sim 70\%$  or less of its theoretical  $\text{CO}_2$  capacity,<sup>39–43</sup> as

aminopolymers can become glassy upon  $\text{CO}_2$  uptake, slowing adsorption kinetics dramatically. When light or heat is applied to the cuvette-reactor, the  $\text{CO}_2$  concentration measured increases significantly corresponding to desorption. Average values of desorbed  $\text{CO}_2$  in these experiments range between 2.25 and 2.80 mmol  $\text{CO}_2$  per g PEI, in line with most literature values for PEI-based sorbents reported between 1 and 3 mmol  $\text{CO}_2$  per g PEI.<sup>39,44–49</sup> The presence of TiN resulted in a 10-fold increase in photo-swing  $\text{CO}_2$  desorption compared to a control sample without TiN (Fig. S4).

Average desorption quantities for three consecutive cycles were measured for dry and humid photo and thermal desorption and summarized in Table 1. In dry conditions, the thermal desorption is more effective than photo-driven desorption, which is expected since the LED only illuminates the bottom part of the sample compared to bulk heating of the entire sample when immersed in the oil bath. Considering that only half of the sample was illuminated, it is impressive that photo-desorbed  $\text{CO}_2$  reached 80% of the thermally desorbed quantity, which we attribute to the high thermal conductivity of TiN ( $22\text{--}29\text{ W m}^{-1}\text{ K}^{-1}$ ) enabling efficient heat conduction throughout the bulk sample.

In humid gas flow settings, photo-swing desorption outperformed the thermal desorption, while, surprisingly, the  $\text{CO}_2$  thermal-swing capacity in humid condition is lower than in dry conditions. This observation is characteristic of the DAC cycling times that are far from thermal equilibrium. For example, Russel-Parks and co-authors showed that PEI's mobility, depending on the humidity level, could require  $>90$  min to equilibrate in humid  $\text{CO}_2$  conditions,<sup>41</sup> which is much longer than the 15 min used in DAC. Under our simulated DAC conditions, the role of humidity can be at least two-fold. First, it is known that  $\text{H}_2\text{O}$  stabilizes carbamate species, thereby freeing an amine binding site for additional interaction with  $\text{CO}_2$ ,<sup>50–52</sup> such that a two-fold increase in  $\text{CO}_2$  capacity is, in principle, possible in the presence of  $\text{H}_2\text{O}$ . Because of this binding

**Table 1** Overview of the  $\text{CO}_2$  desorbed in mmol  $\text{CO}_2$  per g PEI desorbed when exposed to 625 nm light at  $\sim 420\text{ mW cm}^{-2}$  or a thermal oil bath set at  $110^\circ\text{C}$ . Error bars represent the standard deviation across three cycles

	625 nm light	Thermal
Humid	$2.80 \pm 0.03$	$2.52 \pm 0.08$
Dry	$2.25 \pm 0.03$	$2.72 \pm 0.01$

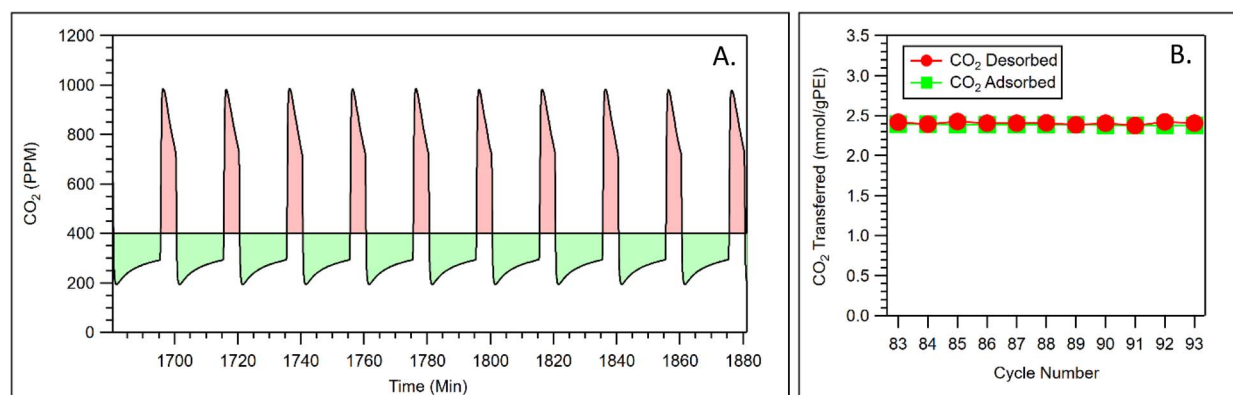


**Fig. 4** (A)  $\text{CO}_2$  concentration (in ppm) during the 83rd and 93rd cycles, last 10 cycles of a cycling series using a dry  $\text{CO}_2$  gas flow. The green-shaded areas represent the 15 min-long adsorption half-cycle and the red-shaded areas are the 5 min-long exposures to the light when an increase in  $\text{CO}_2$  signal is detected. The photo-activated desorption, denoted in red, was initiated using the low-power 625 nm LED set to  $420\text{ mW cm}^{-2}$ . (B)  $\text{CO}_2$  concentrations (in mmol  $\text{CO}_2$  per g PEI) adsorbed and desorbed during the 83rd and 93rd cycles extracted from the integrated areas of the green-shaded and red-shaded areas in (A) associated with an adsorption and a photo-swing desorption step, respectively.





mechanism, the presence of H<sub>2</sub>O also prevents the high degree of polymer crosslinking that occurs in dry conditions linked to a higher polymer mobility than in dry conditions.<sup>51,53–59</sup> Additionally, water has a higher heat capacity (4.2 J g<sup>−1</sup> K<sup>−1</sup>) than amine-impregnated silica (1.1–1.7 J g<sup>−1</sup> K<sup>−1</sup>) such that it can act as a heat sink, further delaying bulk heating.<sup>60,61</sup> In other words, additional energy is necessary to desorb the same amount of CO<sub>2</sub> in humid gas streams, as exemplified by Wurzbacher who measured a 30% CO<sub>2</sub> desorption energy increase between a 20% relative humidity (RH) to a 80% RH gas stream.<sup>62,63</sup> Since the main difference between photo-swing and temperature-swing desorption lies in local vs. bulk heating, we hypothesize that the presence of water—and the distinct heat capacities of TiN, H<sub>2</sub>O, and PEI—impacts the tradeoff between increased polymer mobility (plasticity and CO<sub>2</sub> capacity) and induced thermal “resistance”.<sup>48,64,65</sup>

Consistent with other studies using PEI,<sup>64,66,67</sup> the presence of H<sub>2</sub>O also affects the photo-swing CO<sub>2</sub> desorption kinetics. The difference in the CO<sub>2</sub> desorbed in dry and humid conditions is more pronounced for prolonged light exposures as inferred by Fig. S5. While in dry flow, the peak CO<sub>2</sub> desorption is reached within the first minute of heat or light applied, in the humid system, CO<sub>2</sub> desorption seems to be slower, to exhibit multiple desorption events, and to require close to 2 minutes to reach maximum desorption levels. In the photo-swing process, the trace in Fig. 3C hints to more features, which could be related to localized heating desorbing H<sub>2</sub>O heterogeneously throughout the samples.

### 3.3 Effect of photo-cycling – 93 cycles

Introducing a mechanical shutter mechanism between the LED and the sample, a continuous flow of dry 400 ppm CO<sub>2</sub> gas stream was exposed to the sample for 33 hours, allowing for the measurement of >90 photo-swing adsorption–desorption cycles

over the TiN. Fig. 4A shows the CO<sub>2</sub> evolution during cycle 83 and 93 that are representative of the other cycles during this experiment. The difference of 2.4 vs. 2.18 mmol CO<sub>2</sub> per g PEI recorded during the photo-desorption step in Fig. 2 and 4, respectively in the same experimental conditions is mainly attributed to the slight differences in LED alignment for the two sets of experiments, since photo-activated systems are very sensitive to alignment and focus, as can be seen from Fig. S6. Comparing the amount of CO<sub>2</sub> adsorbed and desorbed per cycle, Fig. 4B shows a 1-to-1 transfer for each of the 10 cycles. Additionally, over 93 cycles, the ratio of CO<sub>2</sub> adsorbed and desorbed remained constant, but the CO<sub>2</sub> capacity decreased by 0.096 mmol CO<sub>2</sub> per g PEI, equivalent to 4% (Fig. S7). Leaching or thermal degradation of the PEI is known to occur, especially in dry and dilute CO<sub>2</sub> flow conditions. Compared to the few reports of cycling experiments in similar conditions, no degradation over 10 cycles and 7% degradation over 25 cycles,<sup>43,49</sup> our value seems promising, especially because the photo-swing approach allows for the optimization of illumination duration or power to prolong the material durability. However, these cycling experiments were performed under simulated conditions in the absence of oxygen. Thanks to the recent overview on the competing kinetic pathways of oxidative degradation of PEI,<sup>68</sup> it is expected that the mild degradation we observe could be accentuated when cycling under real-life operation if oxygen is not purged from the sorbent prior to illumination. Despite mild degradation over 93 cycles, PEI exhibits compatibility with the photo-induced local heating.

### 3.4 Effect of applied light irradiance and wavelength

LEDs with a 385 nm and 625 nm were tested and compared with a broadband light, also referred to as white light. For each LED, the set current was varied according to the LED's range (0–1000 mA for white and red light, 0–700 mA for UV light) and the

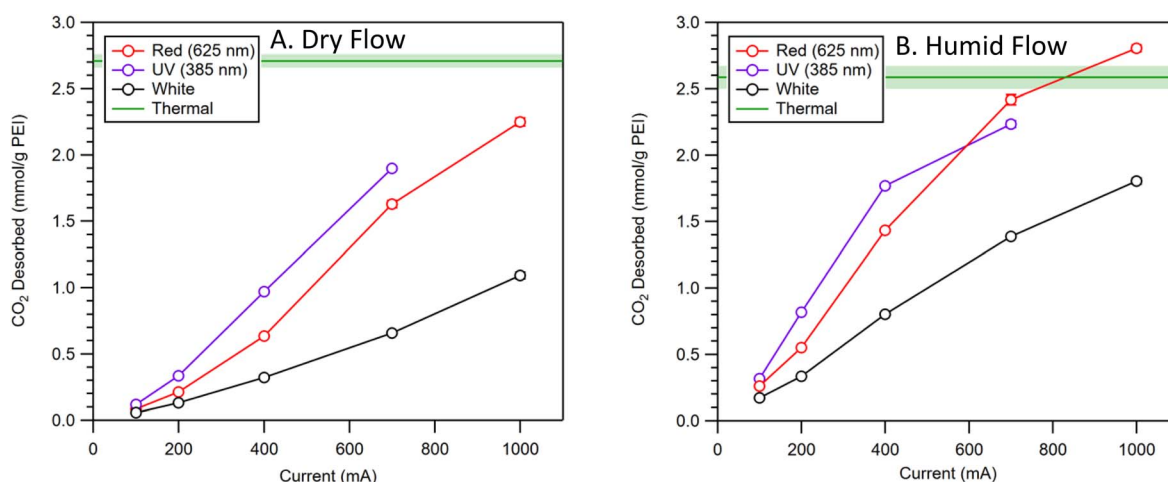


Fig. 5 Measured CO<sub>2</sub> desorption (mmol per g PEI) as a function of set light intensities in dry (A) and humid (B) conditions, with the lines between data points acting as guides to the eye. The sample was exposed to 400 ppm CO<sub>2</sub>/N<sub>2</sub> for 15 min, and to various light sources and intensities (or temperature) for 5 min. Error bars represent the standard deviation of three independent measurements. In both graphs, the green line shows the CO<sub>2</sub> desorbed from bulk heating of the contactor, where the shaded region is representative of the standard deviation over 3 cycles. The standard deviation for the photo-swing desorption was also included in the graphs in the form of error bars that are often smaller than data markers.



associated irradiance ( $10\text{--}420\text{ mW cm}^{-2}$ ), also referred to as power density, was measured and is summarized in Table S1. The amount of  $\text{CO}_2$  was measured under these conditions for dry and humid  $\text{CO}_2$  gas flow, as shown in Fig. 5A and B, respectively. It has been previously shown,<sup>36</sup> that distinguishing between a photothermal and photochemical mechanism based on light power dependence can be challenging. This difficulty arises because a shallow exponential curve, characteristic of a photothermal process, can closely resemble a linear curve, typical of a photochemical process. This similarity is evident in the fit of our results, as illustrated in Fig. S8. However, upon closer examination, the exponential function provides a better fit to our data, particularly in the humid  $\text{CO}_2$  stream case. Based on this observation, we conclude that plasmonic heating is the primary mechanism driving the photo-swing DAC process. Specifically, the local temperature increase caused by light absorption in TiN is proportional to the light power applied to the sample, resulting in  $\text{CO}_2$  release. The white light has the shallowest increase of the 3 LEDs, consistent with a small irradiance value (see Fig. S3) and discontinuous spectrum in the range of interest, 380–750 nm. The UV light desorbs the most  $\text{CO}_2$ , closely followed by the red light, consistent with both, the UV and red wavelengths aligning with TiN's absorbance band. In the humid flow, the overall  $\text{CO}_2$  photo-desorption increases for all three lamps. While the  $\text{CO}_2$  desorption increases similarly to the dry case for the white light, there is an inflexion point  $\sim 400\text{ mA}$  and  $\sim 700\text{ mA}$  for the UV and red light, respectively. This behavior could be indicative of a mass-transfer limited regime, due to efficient  $\text{CO}_2$  desorption being close to the saturation capacity of the PEI system. A competitive mechanism could be a heat transfer limitation of the material system due to illuminating only one contactor half.

## 4. Conclusion

In conclusion, our study shows the potential of photo-swing  $\text{CO}_2$  capture using branched PEI-based contactors enhanced by cost-effective plasmonic TiN and low-power LEDs. Notably, our findings reveal that even with illumination on just one side of the contactor, the photo-swing method achieves comparable  $\text{CO}_2$  desorption levels to traditional thermally driven processes. This exceptional desorption capacity is likely attributed to the localized heating facilitated by plasmonically activated TiN, coupled with its high thermal conductivity, releasing  $>99\%$  of adsorbed  $\text{CO}_2$  in 5 min. Moreover, our extensive cycling experiment, spanning  $>90$  cycles, underscores the remarkable stability of the TiN light absorber and the photothermal durability of the aminopolymer indicating the long-term resilience of these materials in the photo-swing  $\text{CO}_2$  capture process. Compared to existing and emerging DAC technologies, photo-swing DAC paves a way towards a fast process with reduced thermal energy penalties. To accurately assess the true potential of this lab-scale technology as a cost- and energy-competitive DAC solution, we recommend the development of a dedicated sorbent architecture able to maximize the interaction of light with the photo-responsive material and optimize operating

conditions, including light type and applied optical power, to enhance photon-to-desorbed- $\text{CO}_2$  efficiencies.

The implications of our findings offer potential practical solutions to the environmental challenge of carbon removal from the atmosphere. For instance, the light-driven desorption approach could be particularly advantageous in cold climates where the energy efficiency of steam-driven processes is compromised. Furthermore, the application of photo-swing  $\text{CO}_2$  capture in small modular reactors for DAC not only mitigates the cost constraints associated with steam-driven methods but also reduces the initial capital investment required, thereby fostering widespread adoption and utilization of DAC technology. Lastly, our research introduces a promising avenue for enabling reactive capture within aminopolymer systems, historically hindered by  $\text{CO}_2$  slip from the sorbent occurring before requisite catalytic conversion temperatures can be reached ( $>200\text{ }^\circ\text{C}$ ),<sup>69</sup> temperatures which also decompose the polymer. Photocatalysis, however, can lower activation energies and enable low temperature catalysis, offering unprecedented opportunities to leverage mature aminopolymer-based capture media for efficient and sustainable  $\text{CO}_2$  capture and conversion processes.

## Conflicts of interest

There are no conflicts to declare.

## Data availability

The data supporting this article have been included as part of the SI.

Spectroscopy results, photographs of the experimental setup used, reported and measured irradiances for the LEDs used, calculations, baseline measurements relevant to our results, 93 cycles of photo-swing DAC, and fit results can be found in the SI. See DOI: <https://doi.org/10.1039/d5ta02824h>.

## Acknowledgements

This work was authored in part by the National Renewable Energy Laboratory (NREL), operated by Alliance for Sustainable Energy, LLC, for the US Department of Energy (DOE) under contract no. DE-AC36-08GO28308. Development of the photo-desorption equipment, instrumentation, methodology, and wavelength studies was supported by the Laboratory Directed Research and Development (LDRD) Program at NREL. Cycling and durability work was supported by the U.S. DOE, Office of Science, Basic Energy Sciences, Materials Sciences and Engineering Division in response to the DOE National Laboratory Announcement Number LAB 20–2303: Materials and Chemical Sciences Research for Direct Air Capture of Carbon Dioxide. The views expressed in the article do not necessarily represent the views of the DOE or the U.S. Government. The U.S. Government retains and the publisher, by accepting the article for publication, acknowledges that the U.S. Government retains a nonexclusive, paid-up, irrevocable, worldwide license to publish or



reproduce the published form of this work, or allow others to do so, for U.S. Government purposes.

## References

- 1 J.-D. Mathias, J. M. Anderies and M. A. Janssen, On our rapidly shrinking capacity to comply with the planetary boundaries on climate change, *Sci. Rep.*, 2017, 7(1), 42061, DOI: [10.1038/srep42061](#).
- 2 N. McQueen, K. V. Gomes, C. McCormick, K. Blumanthal, M. Pisciotto and J. Wilcox, A review of direct air capture (DAC): scaling up commercial technologies and innovating for the future, *Prog. Energy*, 2021, 3(3), 032001, DOI: [10.1088/2516-1083/abf1ce](#).
- 3 E. M. Agee and A. Orton, An Initial Laboratory Prototype Experiment for Sequestration of Atmospheric CO<sub>2</sub>, *J. Appl. Meteorol. Climatol.*, 2016, 55(8), 1763–1770, DOI: [10.1175/JAMC-D-16-0135.1](#).
- 4 P. Styring, G. Dowson and S. Rackley, Chapter 13 – Direct air capture. in *Negative Emissions Technologies for Climate Change Mitigation*, ed. S. Rackley, G. Andrews, D. Clery, R. De Richter, G. Dowson, P. Knops, W. Li, S. McCord, T. Ming, A. Sewel, *et al.*, Elsevier, 2023, pp. 275–305.
- 5 S. K. S. Boetcher, J. B. Perskin, Y. Maidenberger, M. J. Traum and T. von Hippel, Direct atmospheric cryogenic carbon capture in cold climates, *Carbon Capture Sci. Technol.*, 2023, 8, 100127, DOI: [10.1016/j.ccst.2023.100127](#).
- 6 T. von Hippel, Thermal removal of carbon dioxide from the atmosphere: energy requirements and scaling issues, *Clim. Change*, 2018, 148(4), 491–501, DOI: [10.1007/s10584-018-2208-0](#).
- 7 J. L. Wade, H. Lopez Marques, W. Wang, J. Flory and B. Freeman, Moisture-driven CO<sub>2</sub> pump for direct air capture, *J. Membr. Sci.*, 2023, 685, 121954, DOI: [10.1016/j.memsci.2023.121954](#).
- 8 X. Shi, H. Xiao, K. Kanamori, A. Yonezu, K. S. Lackner and X. Chen, Moisture-Driven CO<sub>2</sub> Sorbents, *Joule*, 2020, 4(8), 1823–1837, DOI: [10.1016/j.joule.2020.07.005](#).
- 9 X. Wang, Y. Chen, W. Xu, A. Lindbråthen, X. Cheng, X. Chen, L. Zhu and L. Deng, Development of high capacity moisture-swing DAC sorbent for direct air capture of CO<sub>2</sub>, *Sep. Purif. Technol.*, 2023, 324, 124489, DOI: [10.1016/j.seppur.2023.124489](#).
- 10 S. Voskian and T. A. Hatton, Faradaic electro-swing reactive adsorption for CO<sub>2</sub> capture, *Energy Environ. Sci.*, 2019, 12(12), 3530–3547, DOI: [10.1039/C9EE02412C](#).
- 11 W. H. Lee, X. Zhang, S. Banerjee, C. W. Jones, M. J. Realff and R. P. Lively, Sorbent-coated carbon fibers for direct air capture using electrically driven temperature swing adsorption, *Joule*, 2023, 7(6), 1241–1259, DOI: [10.1016/j.joule.2023.05.016](#).
- 12 T. Chronopoulos, Y. Fernandez-Diez, M. M. Maroto-Valer, R. Ocone and D. A. Reay, Utilisation Of Microwave Energy for CO<sub>2</sub> Desorption in Post-combustion Carbon Capture Using Solid Sorbents, *Energy Proc.*, 2014, 63, 2109–2115, DOI: [10.1016/j.egypro.2014.11.227](#).
- 13 M. Erguvan and S. Amini, Experimental microwave assisted CO<sub>2</sub> desorption of a solid sorbent in a fluidized bed reactor, *Sep. Purif. Technol.*, 2024, 343, 127062, DOI: [10.1016/j.seppur.2024.127062](#).
- 14 J. Li, Y. Li, C. Li, R. Tu, P. Xie, Y. He and Y. Shi, CO<sub>2</sub> absorption and microwave regeneration with high-concentration TETA nonaqueous absorbents, *Greenh. Gases: Sci. Technol.*, 2022, 12(3), 362–375, DOI: [10.1002/ghg.2148](#).
- 15 A. M. Zito, L. E. Clarke, J. M. Barlow, D. Bím, Z. Zhang, K. M. Ripley, C. J. Li, A. Kummeth, M. E. Leonard, A. N. Alexandrova, *et al.*, Electrochemical Carbon Dioxide Capture and Concentration, *Chem. Rev.*, 2023, 123(13), 8069–8098, DOI: [10.1021/acs.chemrev.2c00681](#).
- 16 H. Li, M. R. Hill, C. Doblin, S. Lim, A. J. Hill and P. Falcaro, Visible Light Triggered CO<sub>2</sub> Liberation from Silver Nanocrystals Incorporated Metal–Organic Frameworks, *Adv. Funct. Mater.*, 2016, 26(27), 4815–4821, DOI: [10.1002/adfm.201600827](#).
- 17 Y. Liao, S.-W. Cao, Y. Yuan, Q. Gu, Z. Zhang and C. Xue, Efficient CO<sub>2</sub> Capture and Photoreduction by Amine-Functionalized TiO<sub>2</sub>, *Chem.–Eur. J.*, 2014, 20(33), 10220–10222, DOI: [10.1002/chem.201403321](#).
- 18 H. Seo, J. Schretter, M. Massen-Hane and T. A. Hatton, Visible Light-Driven CO<sub>2</sub> Capture and Release Using Photoactive Pyranine in Water in Continuous Flow, *J. Am. Chem. Soc.*, 2024, 146(39), 26777–26785, DOI: [10.1021/jacs.4c07278](#).
- 19 V. Juvé, M. F. Cardinal, A. Lombardi, A. Crut, P. Maioli, J. Pérez-Juste, L. M. Liz-Marzán, N. Del Fatti and F. Vallée, Size-Dependent Surface Plasmon Resonance Broadening in Nonspherical Nanoparticles: Single Gold Nanorods, *Nano Lett.*, 2013, 13(5), 2234–2240, DOI: [10.1021/nl400777y](#).
- 20 Z. Y. Pan, J. Zhou, H. Y. Zou, Y. F. Li, P. F. Gao and C. Z. Huang, In situ investigating the size-dependent scattering signatures and sensing sensitivity of single silver nanocube through a multi-model approach, *J. Colloid Interface Sci.*, 2021, 584, 253–262, DOI: [10.1016/j.jcis.2020.09.121](#).
- 21 P. Patsalas, N. Kalfagiannis and S. Kassavetis, Optical Properties and Plasmonic Performance of Titanium Nitride, *Materials*, 2015, 8(6), 3128–3154.
- 22 A. Campos, N. Troc, E. Cottancin, M. Pellarin, H.-C. Weissker, J. Lermé, M. Kociak and M. Hillenkamp, Plasmonic quantum size effects in silver nanoparticles are dominated by interfaces and local environments, *Nat. Phys.*, 2019, 15(3), 275–280, DOI: [10.1038/s41567-018-0345-z](#).
- 23 A. A. Barragan, S. Hanukovich, K. Bozhilov, S. S. R. K. C. Yamijala, B. M. Wong, P. Christopher and L. Mangolini, Photochemistry of Plasmonic Titanium Nitride Nanocrystals, *J. Phys. Chem. C*, 2019, 123(35), 21796–21804, DOI: [10.1021/acs.jpcc.9b06257](#).
- 24 U. Guler, S. Suslov, A. V. Kildishev, A. Boltasseva and V. M. Shalae, Colloidal Plasmonic Titanium Nitride Nanoparticles: Properties and Applications, *Nanophotonics*, 2015, 4(3), 269–276, DOI: [10.1515/nanoph-2015-0017](#).



- 25 A. Catellani and A. Calzolari, Plasmonic properties of refractory titanium nitride, *Phys. Rev. B*, 2017, **95**(11), 115145, DOI: [10.1103/PhysRevB.95.115145](https://doi.org/10.1103/PhysRevB.95.115145).
- 26 W.-P. Guo, R. Mishra, C.-W. Cheng, B.-H. Wu, L.-J. Chen, M.-T. Lin and S. Gwo, Titanium Nitride Epitaxial Films as a Plasmonic Material Platform: Alternative to Gold, *ACS Photonics*, 2019, **6**(8), 1848–1854, DOI: [10.1021/acsp Photonics.9b00617](https://doi.org/10.1021/acsp Photonics.9b00617).
- 27 M. C. Freyman, Z. Huang, D. Ravikumar, E. B. Duoss, Y. Li, S. E. Baker, S. H. Pang and J. A. Schaidle, Reactive CO<sub>2</sub> capture: A path forward for process integration in carbon management, *Joule*, 2023, **7**(4), 631–651, DOI: [10.1016/j.joule.2023.03.013](https://doi.org/10.1016/j.joule.2023.03.013).
- 28 P. Eisenberger, E. W. Ping and M. Sakwa-novak, *Novel Composition Of Matter & Carbon Dioxide Capture Systems*, MX, 2023.
- 29 M. E. Potter, S. H. Pang and C. W. Jones, Adsorption Microcalorimetry of CO<sub>2</sub> in Confined Aminopolymers, *Langmuir*, 2017, **33**(1), 117–124, DOI: [10.1021/acs.langmuir.6b03793](https://doi.org/10.1021/acs.langmuir.6b03793).
- 30 T. C. Drage, A. Arenillas, K. M. Smith and C. E. Snape, Thermal stability of polyethylenimine based carbon dioxide adsorbents and its influence on selection of regeneration strategies, *Microporous Mesoporous Mater.*, 2008, **116**(1), 504–512, DOI: [10.1016/j.micromeso.2008.05.009](https://doi.org/10.1016/j.micromeso.2008.05.009).
- 31 A. Heydari-Gorji and A. Sayari, Thermal, Oxidative, and CO<sub>2</sub>-Induced Degradation of Supported Polyethylenimine Adsorbents, *Ind. Eng. Chem. Res.*, 2012, **51**(19), 6887–6894, DOI: [10.1021/ie3003446](https://doi.org/10.1021/ie3003446).
- 32 L. Zhou, D. F. Swearer, C. Zhang, H. Robotjazi, H. Zhao, L. Henderson, L. Dong, P. Christopher, E. A. Carter, P. Nordlander, *et al.*, Quantifying hot carrier and thermal contributions in plasmonic photocatalysis, *Science*, 2018, **362**(6410), 69–72, DOI: [10.1126/science.aat6967](https://doi.org/10.1126/science.aat6967).
- 33 Y. Sivan, J. Baraban, I. W. Un and Y. Dubi, Comment on “Quantifying hot carrier and thermal contributions in plasmonic photocatalysis”, *Science*, 2019, **364**(6439), eaaw9367, DOI: [10.1126/science.aaw9367](https://doi.org/10.1126/science.aaw9367).
- 34 X. Zhang, X. Li, M. E. Reish, D. Zhang, N. Q. Su, Y. Gutiérrez, F. Moreno, W. Yang, H. O. Everitt and J. Liu, Plasmon-Enhanced Catalysis: Distinguishing Thermal and Nonthermal Effects, *Nano Lett.*, 2018, **18**(3), 1714–1723, DOI: [10.1021/acs.nanolett.7b04776](https://doi.org/10.1021/acs.nanolett.7b04776).
- 35 M. Thangamuthu, T. V. Raziman, O. J. F. Martin and J. Tang, Review—Origin and Promotional Effects of Plasmonics in Photocatalysis, *J. Electrochem. Soc.*, 2022, **169**(3), 036512, DOI: [10.1149/1945-7111/ac5c97](https://doi.org/10.1149/1945-7111/ac5c97).
- 36 G. Baffou, I. Bordacchini, A. Baldi and R. Quidant, Simple experimental procedures to distinguish photothermal from hot-carrier processes in plasmonics, *Light: Sci. Appl.*, 2020, **9**(1), 108, DOI: [10.1038/s41377-020-00345-0](https://doi.org/10.1038/s41377-020-00345-0).
- 37 G. Baffou, P. Berto, E. Bermúdez Ureña, R. Quidant, S. Monneret, J. Polleux and H. Rigneault, Photoinduced Heating of Nanoparticle Arrays, *ACS Nano*, 2013, **7**(8), 6478–6488, DOI: [10.1021/nn401924n](https://doi.org/10.1021/nn401924n).
- 38 A. O. Govorov, W. Zhang, T. Skeini, H. Richardson, J. Lee and N. A. Kotov, Gold nanoparticle ensembles as heaters and actuators: melting and collective plasmon resonances, *Nanoscale Res. Lett.*, 2006, **1**(1), 84, DOI: [10.1007/s11671-006-9015-7](https://doi.org/10.1007/s11671-006-9015-7).
- 39 J. R. Hoffman, A. E. Baumann and C. M. Stafford, Thickness dependent CO<sub>2</sub> adsorption of poly(ethyleneimine) thin films for direct air capture, *Chem. Eng. J.*, 2024, **481**, 148381, DOI: [10.1016/j.cej.2023.148381](https://doi.org/10.1016/j.cej.2023.148381).
- 40 R. Sanz, G. Calleja, A. Arencibia and E. S. Sanz-Pérez, CO<sub>2</sub> Uptake and Adsorption Kinetics of Pore-Expanded SBA-15 Double-Functionalized with Amino Groups, *Energy Fuels*, 2013, **27**(12), 7637–7644, DOI: [10.1021/ef4015229](https://doi.org/10.1021/ef4015229).
- 41 G. A. Russell-Parks, N. Leick, M. A. T. Marple, N. A. Strange, B. G. Trewyn, S. H. Pang and W. A. Braunecker, Fundamental Insight into Humid CO<sub>2</sub> Uptake in Direct Air Capture Nanocomposites Using Fluorescence and Portable NMR Relaxometry, *J. Phys. Chem. C*, 2023, **127**(31), 15363–15374, DOI: [10.1021/acs.jpcc.3c03653](https://doi.org/10.1021/acs.jpcc.3c03653).
- 42 X. Qiu, S. Wang and S. Chen, The self-assembly of dialdehyde-cellulose-nanofiber-based hydrogels with high compression resilience, *Cellulose*, 2022, **29**(10), 5645–5658, DOI: [10.1007/s10570-022-04605-7](https://doi.org/10.1007/s10570-022-04605-7).
- 43 L. B. Hamdy, A. Gougsa, W. Y. Chow, J. E. Russell, E. García-Díez, V. Kulakova, S. Garcia, A. R. Barron, M. Taddei and E. Andreoli, Overcoming mass transfer limitations in cross-linked polyethylenimine-based adsorbents to enable selective CO<sub>2</sub> capture at ambient temperature, *Mater. Adv.*, 2022, **3**(7), 3174–3191, DOI: [10.1039/D1MA01072G](https://doi.org/10.1039/D1MA01072G), DOI: [10.1039/D1MA01072G](https://doi.org/10.1039/D1MA01072G).
- 44 A. Goepfert, M. Czaun, G. K. Surya Prakash and G. A. Olah, Air as the renewable carbon source of the future: an overview of CO<sub>2</sub> capture from the atmosphere, *Energy Environ. Sci.*, 2012, **5**(7), 7833–7853, DOI: [10.1039/C2EE21586A](https://doi.org/10.1039/C2EE21586A).
- 45 X. Xu, C. Song, J. M. Andrésen, B. G. Miller and A. W. Scaroni, Preparation and characterization of novel CO<sub>2</sub> “molecular basket” adsorbents based on polymer-modified mesoporous molecular sieve MCM-41, *Microporous Mesoporous Mater.*, 2003, **62**(1), 29–45, DOI: [10.1016/S1387-1811\(03\)00388-3](https://doi.org/10.1016/S1387-1811(03)00388-3).
- 46 C.-H. Yu, C.-H. Huang and C.-S. Tan, A Review of CO<sub>2</sub> Capture by Absorption and Adsorption, *Aerosol Air Qual. Res.*, 2012, **12**(5), 745–769, DOI: [10.4209/aaqr.2012.05.0132](https://doi.org/10.4209/aaqr.2012.05.0132).
- 47 E. S. Sanz-Pérez, C. R. Murdock, S. A. Didas and C. W. Jones, Direct Capture of CO<sub>2</sub> from Ambient Air, *Chem. Rev.*, 2016, **116**(19), 11840–11876, DOI: [10.1021/acs.chemrev.6b00173](https://doi.org/10.1021/acs.chemrev.6b00173).
- 48 G. Rim, P. Priyadarshini, M. Song, Y. Wang, A. Bai, M. J. Realff, R. P. Lively and C. W. Jones, Support Pore Structure and Composition Strongly Influence the Direct Air Capture of CO<sub>2</sub> on Supported Amines, *J. Am. Chem. Soc.*, 2023, **145**(13), 7190–7204, DOI: [10.1021/jacs.2c12707](https://doi.org/10.1021/jacs.2c12707).
- 49 Y. J. Min, A. Ganesan, M. J. Realff and C. W. Jones, Direct Air Capture of CO<sub>2</sub> Using Poly(ethyleneimine)-Functionalized Expanded Poly(tetrafluoroethylene)/Silica Composite Structured Sorbents, *ACS Appl. Mater. Interfaces*, 2022, **14**(36), 40992–41002, DOI: [10.1021/acsami.2c11143](https://doi.org/10.1021/acsami.2c11143).





- 50 D. D. Miller, J. Yu and S. S. C. Chuang, Unraveling the Structure and Binding Energy of Adsorbed CO<sub>2</sub>/H<sub>2</sub>O on Amine Sorbents, *J. Phys. Chem. C*, 2020, **124**(45), 24677–24689, DOI: [10.1021/acs.jpcc.0c04942](https://doi.org/10.1021/acs.jpcc.0c04942).
- 51 J. Hack, N. Maeda and D. M. Meier, Review on CO<sub>2</sub> Capture Using Amine-Functionalized Materials, *ACS Omega*, 2022, **7**(44), 39520–39530, DOI: [10.1021/acsomega.2c03385](https://doi.org/10.1021/acsomega.2c03385).
- 52 K. Li, J. D. Kress and D. S. Mebane, The Mechanism of CO<sub>2</sub> Adsorption under Dry and Humid Conditions in Mesoporous Silica-Supported Amine Sorbents, *J. Phys. Chem. C*, 2016, **120**(41), 23683–23691, DOI: [10.1021/acs.jpcc.6b08808](https://doi.org/10.1021/acs.jpcc.6b08808).
- 53 A. Holewinski, M. A. Sakwa-Novak and C. W. Jones, Linking CO<sub>2</sub> Sorption Performance to Polymer Morphology in Aminopolymer/Silica Composites through Neutron Scattering, *J. Am. Chem. Soc.*, 2015, **137**(36), 11749–11759, DOI: [10.1021/jacs.5b06823](https://doi.org/10.1021/jacs.5b06823).
- 54 W. C. Wilfong, C. S. Srikanth and S. S. C. Chuang, *In Situ* ATR and DRIFTS Studies of the Nature of Adsorbed CO<sub>2</sub> on Tetraethylenepentamine Films, *ACS Appl. Mater. Interfaces*, 2014, **6**(16), 13617–13626, DOI: [10.1021/am5031006](https://doi.org/10.1021/am5031006).
- 55 H.-J. Kim, W. Chaikittisilp, K.-S. Jang, S. A. Didas, J. R. Johnson, W. J. Koros, S. Nair and C. W. Jones, Aziridine-Functionalized Mesoporous Silica Membranes on Polymeric Hollow Fibers: Synthesis and Single-Component CO<sub>2</sub> and N<sub>2</sub> Permeation Properties, *Ind. Eng. Chem. Res.*, 2015, **54**(16), 4407–4413, DOI: [10.1021/ie503781u](https://doi.org/10.1021/ie503781u).
- 56 J. J. Lee, C.-H. Chen, D. Shimon, S. E. Hayes, C. Sievers and C. W. Jones, Effect of Humidity on the CO<sub>2</sub> Adsorption of Tertiary Amine Grafted SBA-15, *J. Phys. Chem. C*, 2017, **121**(42), 23480–23487, DOI: [10.1021/acs.jpcc.7b07930](https://doi.org/10.1021/acs.jpcc.7b07930).
- 57 S. A. Didas, M. A. Sakwa-Novak, G. S. Foo, C. Sievers and C. W. Jones, Effect of Amine Surface Coverage on the Co-Adsorption of CO<sub>2</sub> and Water: Spectral Deconvolution of Adsorbed Species, *J. Phys. Chem. Lett.*, 2014, **5**(23), 4194–4200, DOI: [10.1021/jz502032c](https://doi.org/10.1021/jz502032c).
- 58 M. E. Potter, K. M. Cho, J. J. Lee and C. W. Jones, Role of Alumina Basicity in CO<sub>2</sub> Uptake in 3-Aminopropylsilyl-Grafted Alumina Adsorbents, *ChemSusChem*, 2017, **10**(10), 2192–2201, DOI: [10.1002/cssc.201700115](https://doi.org/10.1002/cssc.201700115).
- 59 R. Kumar, M. Bandyopadhyay, M. Pandey and N. Tsunogi, Amine-impregnated nanoarchitectonics of mesoporous silica for capturing dry and humid 400 ppm carbon dioxide: A comparative study, *Microporous Mesoporous Mater.*, 2022, **338**, 111956, DOI: [10.1016/j.micromeso.2022.111956](https://doi.org/10.1016/j.micromeso.2022.111956).
- 60 M. W. McKittrick and C. W. Jones, Toward Single-Site Functional Materials Preparation of Amine-Functionalized Surfaces Exhibiting Site-Isolated Behavior, *Chem. Mater.*, 2003, **15**(5), 1132–1139, DOI: [10.1021/cm020952z](https://doi.org/10.1021/cm020952z).
- 61 W. Li, P. Bollini, S. A. Didas, S. Choi, J. H. Drese and C. W. Jones, Structural Changes of Silica Mesocellular Foam Supported Amine-Functionalized CO<sub>2</sub> Adsorbents Upon Exposure to Steam, *ACS Appl. Mater. Interfaces*, 2010, **2**(11), 3363–3372, DOI: [10.1021/am100786z](https://doi.org/10.1021/am100786z).
- 62 J. A. Wurzbacher, C. Gebald and A. Steinfeld, Separation of CO<sub>2</sub> from air by temperature-vacuum swing adsorption using diamine-functionalized silica gel, *Energy Environ. Sci.*, 2011, **4**(9), 3584–3592, DOI: [10.1039/C1EE01681D](https://doi.org/10.1039/C1EE01681D).
- 63 R. P. Wijesiri, G. P. Knowles, H. Yeasmin, A. F. A. Hoadley and A. L. Chaffee, Desorption Process for Capturing CO<sub>2</sub> from Air with Supported Amine Sorbent, *Ind. Eng. Chem. Res.*, 2019, **58**(34), 15606–15618, DOI: [10.1021/acs.iecr.9b03140](https://doi.org/10.1021/acs.iecr.9b03140).
- 64 Y. Wang, G. Rim, M. Song, H. E. Holmes, C. W. Jones and R. P. Lively, Cold Temperature Direct Air CO<sub>2</sub> Capture with Amine-Loaded Metal–Organic Framework Monoliths, *ACS Appl. Mater. Interfaces*, 2024, **16**(1), 1404–1415, DOI: [10.1021/acsami.3c13528](https://doi.org/10.1021/acsami.3c13528).
- 65 G. Rim, F. Kong, M. Song, C. Rosu, P. Priyadarshini, R. P. Lively and C. W. Jones, Sub-Ambient Temperature Direct Air Capture of CO<sub>2</sub> using Amine-Impregnated MIL-101(Cr) Enables Ambient Temperature CO<sub>2</sub> Recovery, *JACS Au*, 2022, **2**(2), 380–393, DOI: [10.1021/jacsau.1c00414](https://doi.org/10.1021/jacsau.1c00414).
- 66 P. Priyadarshini, G. Rim, C. Rosu, M. Song and C. W. Jones, Direct Air Capture of CO<sub>2</sub> Using Amine/Alumina Sorbents at Cold Temperature, *ACS Environ. Au*, 2023, **3**(5), 295–307, DOI: [10.1021/acsenvironau.3c00010](https://doi.org/10.1021/acsenvironau.3c00010).
- 67 E. R. Monazam, R. W. Breault, D. J. Fauth, L. J. Shadle and S. Bayham, Insights into the Adsorption of Carbon Dioxide in the Presence of Water Vapor Utilizing a Low Molecular Weight Polyethylenimine-Impregnated CARIAct Silica Sorbent, *Ind. Eng. Chem. Res.*, 2017, **56**(32), 9054–9064, DOI: [10.1021/acs.iecr.7b01271](https://doi.org/10.1021/acs.iecr.7b01271).
- 68 S. Li, Y. Guta, M. F. Calegari Andrade, E. Hunter-Sellars, A. Maiti, A. J. Varni, P. Tang, C. Sievers, S. H. Pang and C. W. Jones, Competing Kinetic Consequences of CO<sub>2</sub> on the Oxidative Degradation of Branched Poly(ethylenimine), *J. Am. Chem. Soc.*, 2024, **146**(41), 28201–28213, DOI: [10.1021/jacs.4c08126](https://doi.org/10.1021/jacs.4c08126).
- 69 J. M. Crawford, M. J. Rasmussen, W. W. McNeary, S. Halingstad, S. C. Hayden, N. S. Dutta, S. H. Pang and M. Y. Matthew, High Selectivity Reactive Carbon Dioxide Capture over Zeolite Dual-Functional Materials, *ACS Catal.*, 2024, **14**(11), 8541–8548, DOI: [10.1021/acscatal.4c01340](https://doi.org/10.1021/acscatal.4c01340).

